

Spin-charge interplay in antiferromagnetic LSCO studied by the muons, neutrons, and ARPES techniques

Gil Drachuck,¹ Elia Razzoli,^{2,3} Galina Bazalitski,¹ Amit Kanigel,¹ Christof Niedermayer,⁴ Ming Shi,² and Amit Keren¹

¹*Department of Physics, Technion - Israel Institute of Technology, Haifa, 32000, Israel*

²*Swiss Light Source, Paul Scherrer Institute, CH-5232 Villigen PSI, Switzerland*

³*Dpartement de Physique and Fribourg Center for Nanomaterials, Universit de Fribourg, CH-1700 Fribourg, Switzerland*

⁴*Laboratory for Neutron Scattering, Paul Scherrer Institute, CH-5232 Villigen PSI, Switzerland*
(Dated: February 28, 2014)

Exploring whether a spin density wave (SDW) is responsible for the charge excitations gap in the high-temperature superconducting cuprates is difficult, since the region of the phase diagram where the magnetic properties are clearly exposed is different from the region where the band dispersion is visible. On the one hand, long range magnetic order disappears as doping approaches 2% from below, hindering our ability to perform elastic neutron scattering (ENS). On the other hand, cuprates become insulating at low temperature when the doping approaches 2% from above, thus restricting angle-resolved photoemission spectroscopy (ARPES). In fact, ARPES data for samples with doping lower than 3% are rare and missing the quasiparticle peaks in the energy distribution curves (EDCs) [1] [2]. The main problem is the high resistivity of extremely underdoped samples, which is detrimental to ARPES due to charging effects. Nevertheless, the resistivity of $\text{La}_{2-x}\text{Sr}_x\text{CuO}_4$ [LSCO] as a function of temperature, at 2% doping, has a broad minimum around 100 K [3]. This minimum opens a window for both experiments. By preparing a series of LSCO single crystals with ~ 0.2 - 0.3% doping steps around 2%, we managed to find one to which both techniques apply. This allows us to explore the cross talk between the magnetic and electronic properties of the material.

The series of samples are first characterized by muon spin rotation (μSR). In Fig. 1a we show the muon spin rotation frequency as a function of temperature for all the crystals. In samples with doping equal to or less than 2%, the oscillation starts at temperatures on the order of 100 K. At 2%, there is a sharp transition from the antiferromagnetic long range order to the spin glass state where the same oscillations appear only at temperatures on the order of 10 K [4]. More details of the μSR characterization of the samples are given below and in the supplementary material. We perform the ENS and ARPES measurements on a sample with $x = 1.92\%$ (red rhombuses) which is antiferromagnetic with a Néel temperature $T_N = 140$ K. Fig. 1b shows the ARPES intensity map near the Fermi level (E_F) in the second Brillouin Zone (BZ), measured along cuts parallel to cut 1 and 2 shown in the figure. The high intensities represent the underlying Fermi surface (FS) and has the morphology of the FS in more doped LSCO [5] and other cuprates. Most of the intensity is centered around the zone diag-

onal. This suggests the presence of gapped electronic excitations in the off-diagonal $(0, \pi)$ region. Similar results were obtained at a higher doping level of $x = 3 - 8\%$ [6].

Figure 1c depicts ENS for the same sample at 3 K. The scans are performed in a narrow range in the reciprocal lattice space centered around the $(1, -1)$ point, in the standard tetragonal ARPES units of π/a . The scanned area of the ENS experiment is presented on the BZ of the ARPES experiment by the small inset in Fig. 1b. Two incommensurate peaks are present in the center of the figure. Such incommensurate peaks occur when, on top of the main magnetic order, the system develops spin modulations (stripes) running in diagonal to the bond directions (diagonal stripes). The stripes and commensurate scattering observed in our sample are in agreement with previous reports for low doping LSCO [7, 8], and are discussed further below.

In Fig. 2a-h, we show the temperature dependence of ARPES data in the vicinity of point III along cut 3 in Fig. 1b. All spectra are divided by resolution broadened Fermi-Dirac distribution at the nominal temperature. Data analysis by the Lucy-Richardson deconvolution method [9] is discussed in the supplementary material. At high temperatures ($T > 50$ K), the dispersive peak crosses E_F as clearly seen in Fig. 2a. In contrast, at low temperatures ($T < 45$ K) there is a gap in the electronic spectra, *i.e.* the peak position at k_F stays below E_F . A similar gap exists in LSCO up to 8% doping [6], in LBCO at 4% [2], in the electron doped compound [10], and in Bi2212 [11], and also in simulations where inhomogeneous SDW and superconductivity coexist [12]. EDCs extracted from Fig. 2a-h, at k_F given by point III of Fig. 1b, are plotted in Fig. 2i. The solid lines are guides to the eye. At temperatures above 45 K, the peak is at E_F . However, below this temperature the peaks are clearly below E_F , indicating the presence of a gap. Another important aspect of these EDCs is the fact that at all low temperatures, E_F is not in the middle of the gap, namely, the intensity of the spectra immediately above E_F is lower than at E_F . This could be an analysis artifact due to the division by the resolution broadened Fermi-Dirac function [13] or indicate that the particle-hole symmetry is broken. Particle-hole asymmetry toward the diagonal region in the non-superconducting phase [14], and in the

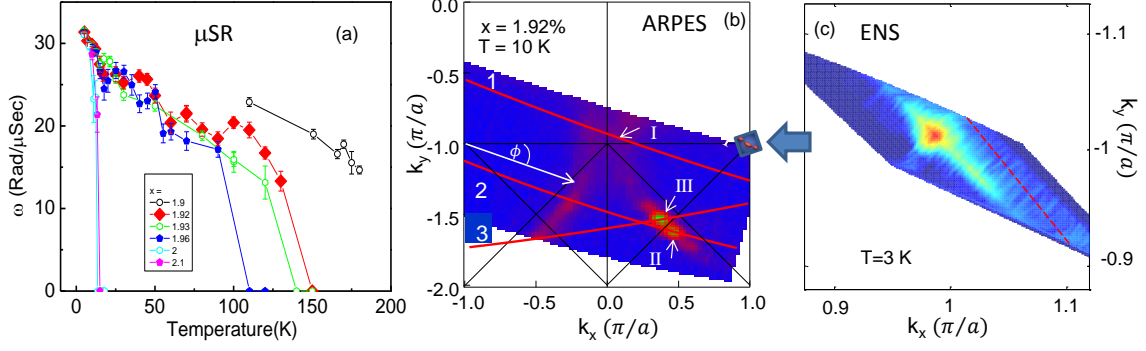


FIG. 1: (a) muon spin rotation frequency as a function of temperature for LSCO single crystals with different x values. At $x = 2\%$ there is a clear transition from an antiferromagnetic to a spin-glass ground states. The data in the rest of this paper is from the $x=1.92\%$ sample which is in the antiferromagnetic phase. (b) Low energy ARPES data in the second Brillouin Zone. The red lines 1, 2 show cuts on which data was collected. Line 3 is the cut on which temperature dependence data is presented in Fig. 2. Point I, II, and III mark points where EDCs are extracted. The inset at $\mathbf{k} = (1, -1)$ is an illustration of the location of the commensurate and incommensurate magnetic peaks. (c) Elastic neutron scattering measurements at 3 K around a magnetic reciprocal lattice vector showing two incommensurate peaks. The red lines depicts the measurements scan direction.

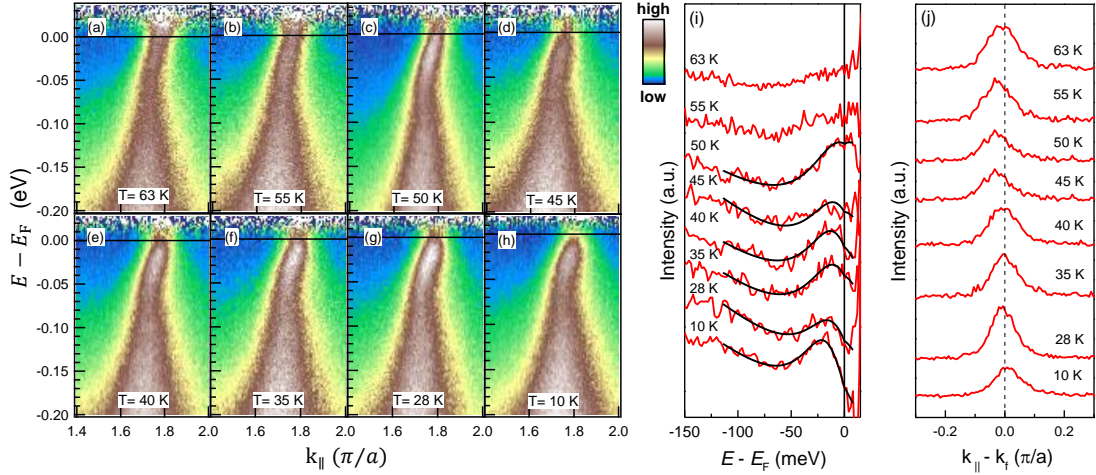


FIG. 2: (a-h) ARPES spectra along a cut given by line 3 in Fig. 1. The spectra are divided into resolution broadened Fermi-Dirac distribution. At high T the spectrum crosses the Fermi energy. At low T it does not. (i) EDCs at the Fermi momentum of point III in Fig. 1b for different temperatures. The solid lines are guides to the eye. At 10 K the peak is clearly below the Fermi energy. $\Delta(T)$ is presented in Fig. 4c. (j) MDC at E_F as a function of temperature showing that k_F in the diagonal region is temperature independent.

off-diagonal region [15], was found previously. However, it is very difficult to distinguish between the two options in our sample with extremely low carrier concentration.

Another parameter relevant for understanding the mechanism by which this diagonal gap opens is the temperature dependence of k_F . This is explored by extracting the momentum dispersion curve (MDC) at E_F from Fig. 2a-h, as presented in Fig. 2j. The peak position fluctuates somewhat around a constant value as the temperature is lowered, indicating that $k_F = 0.63(\pi/a)$ along the diagonal is temperature-independent. Therefore, the high intensity curves in Fig. 1b represents the FS.

The evolution of the gap around the FS is shown in Fig. 3a-b for 10 and 100 K. The spectra marked I and II in Fig. 3a are EDCs at the \mathbf{k}_F of points I and II in Fig. 1b. The spectrum in between correspond to \mathbf{k}_F between point I and II. EDCs shown in Fig. 3b are from similar point along the FS. In the off-diagonal region, there is no spectral weight at E_F for both temperatures, indicating that the off-diagonal gap opens at a temperature higher than 100 K. In the diagonal region, there is high spectral weight at 100 K, but not at 10 K. Thus at 100 K we observe a Fermi arc [16], while at 10 K a gap appears all around the FS.

Finally, in Fig. 4 we present a summary of parameters extracted from all three techniques. Fig. 4a shows the temperature dependence of the muon rotation frequency and magnetic volume fraction. The inset represents a fit of a three-component model, with one frequency, to the μ SR data at different temperatures. More details are available in the supplementary material. The magnetic parameters grow upon cooling, saturate between 50 and 25 K, and grow again at lower temperatures. The temperature $T_f = 25$ K was associated with hole freezing into one dimensional domain walls [4, 17]. The restriction of the charge motion below T_f must be intimately related to the opening of the nodal gap.

Fig. 4b shows the commensurate and the incommensurate scattering intensity. The inset shows the raw data along the red diagonal line in Fig. 1c (in orthorhombic units). As the temperature is raised, the incommensurate intensity decreases until it disappears at $T_f = 30$ K. The commensurate intensity peaks at 25 K, just when the muon oscillation change its behavior, and vanishes at $T_N = 130$ K. Our ENS temperature dependence results and incommensurability parameter (in tetragonal units) $\delta = 0.027(\pi/a)$ are in good agreement with previously reported data [8]. While the ENS data is well understood in terms of a spiral ground state [18], its relation to the gap is still mysterious, since the nesting condition $k_F + \delta = \frac{\sqrt{2}\pi}{2a}$ is not fulfilled in our sample.

The diagonal gaps at k_F , Δ , are determined from the peak in the EDCs of Fig. 2i and presented in Fig. 4c as a function of temperature. Very similar gap values are found using the Lucy-Richardson de-convolutions method (see supplementary material) [9]. The gap opens at 50 K. The major observations in this figure are: I) the diagonal gap opens only when the commensurate moment

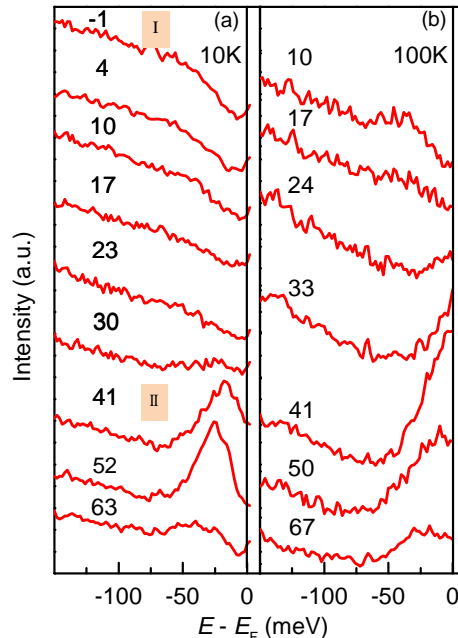


FIG. 3: (a) EDCs at different \mathbf{k}_F along the FS in two different temperatures. The fermi surface angle ϕ is indicated above each EDC. Spectra I and II are taken at the \mathbf{k} of point I and II in Fig. 1b which are defined by the crossing point between the red lines 1 and 2 and the FS. The other EDCs are from the crossing points in between. At 10K a gap is observed all around the FS. $\Delta(\phi)$ is presented in the inset of Fig. 4c. (b) Similar EDCs at 100 K. In this case a gap is observed only in the off diagonal region.

is nearly at its full value. II) the diagonal gap opens when the incommensurate moment is not detectable by ENS. The angular dependence of the gaps is presented in the inset of Fig. 4c; the angle ϕ is defined in Fig. 1b,. When a peak is absent, the gap is taken from the change of slope in the EDCs. $\Delta(\phi)$ is in agreement with previous measurements for 3 to 8% dopings [6].

On the basis of weak coupling theory, Berg *et al.* [19] argued that the commensurate part of the SDW can open a diagonal gap only if the moment is larger than a critical value. However, the opening of the gap will be accompanied by a shift in k_F . The effect of the incommensurate part of the SDW depends on the properties of time reversal followed by translation symmetry, which can be broken or unbroken. In the unbroken case a nodal gap will open when the perturbation exceeds a critical value. Both these options do not agree with our data. In the broken symmetry case, a nodal gap can open for arbitrarily small perturbation with no impact on k_F . This option is in agreement with our measurements and bares important information on the symmetries of the ground

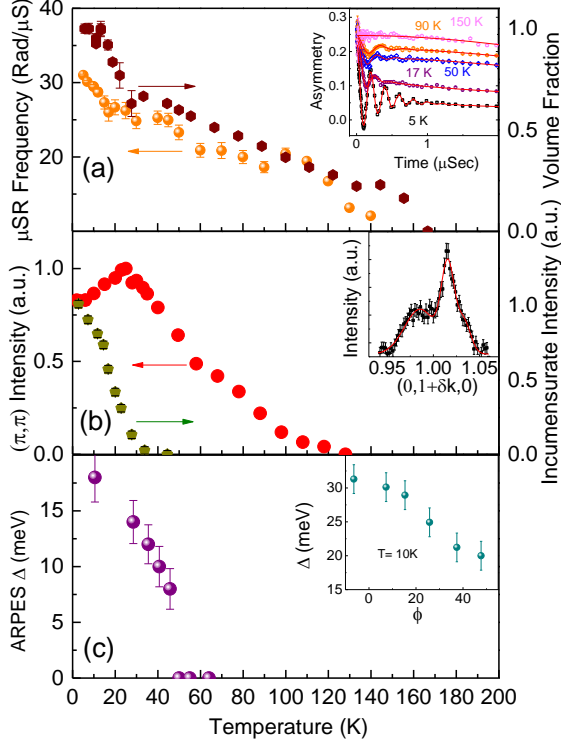


FIG. 4: A summary of experimental parameters from all three techniques. (a) Muon rotation frequency and the magnetic volume fraction of the sample as a function of temperature taken from a fit to a three Lorentzians model (see supplementary material). The inset shows raw data and the fit quality for the x=1.92% sample. (b) Commensurate and incommensurate elastic neutron scattering intensity. The inset is the intensity versus k along the neutron scattering cut in Fig. 1c. (c) ARPES diagonal gap Δ at k_F , as obtained from the peaks in Fig. 2i, versus temperature. The inset shows the angular dependence of the gap $\Delta(\phi)$.

state. Another possibility is that the gap is of the superconducting type, which maintains particle-hole symmetry and keeps k_F fixed. This option would mean that the cuprates have a superconducting gap in the AFM phase.

To summarize, we detect a nodal gap in the AFM phase of $\text{La}_{2-x}\text{Sr}_x\text{CuO}_4$. The gap opens well below T_N and a bit above the temperature where incommensurate SDW is detected. This finding puts strong restrictions on the origin of the nodal gap.

I. SUPPLEMENTARY MATERIAL

A. μ SR

The experiment was carried out at PSI on the GPS beam line. We fit the muon polarization as a function of

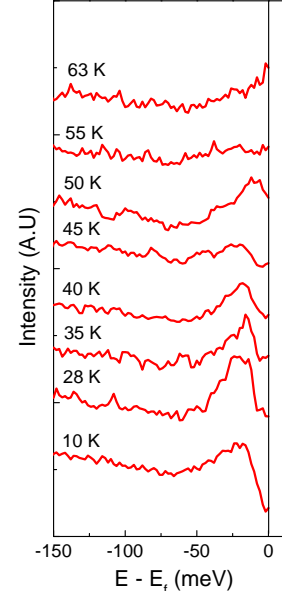


FIG. 5: The same data as in Fig. 2i but analyzed using the Lucy-Richardson deconvolution method [9].

time to

$$P_z(t) = (1 - V_m) e^{-\frac{1}{2} D^2 t^2} + V_m \left[p \times e^{-(R_1 t)^{b_1}} + (1 - p) \times e^{-(R_2 t)^{b_2}} \cos(\omega t + \phi) \right] + P_{Bg}$$

where ω is the muon rotation angular frequency, V_m stands for the magnetic volume fraction, p is the amplitude of the rotating signal resulting from the angle between the muon spin and the internal field, D , R_1 and R_2 are relaxation rates, b_1 and b_2 are stretching exponents, and P_{Bg} is the background polarization from muon that missed the sample. We could fit the data well with $b_1 = 0.5$ and $b_2 = 1$ for most of the temperatures. Between $T = 25$ K to 50 K we allowed freedom in their values to achieve an optimal fit.

B. ARPES

The experiment was done in PSI using conditions similar to those in Ref. [20]. Charging tests have been carried out by varying the photon flux. No charging was found. In addition, after performing the high temperature measurements, the sample was cooled again and the results at 10 K were reproducible. We examined the surface with LEED at each temperature and no degeneration or reconstruction was found during the measurements.

It should be pointed out that in ARPES the incoming light warms the surface and there could be a few degrees difference between the temperature of the surface from which electrons are ejected and the temperature of the cold figure which we quote in the paper.

EDCs obtained by LRM are depicted in Fig. 5.

C. Neutron diffraction

The neutron diffraction experiments were carried out at Paul Scherrer Institute (SINQ, PSI). The crystal was mounted on an aluminium sample holder with the \hat{c} perpendicular to the neutron beam; $(1, 0, 0) - (0, 1, 0)$ scattering plane. The collimation was $80'-40'-80'$. Beryllium filter was placed before the analyzer to remove higher order neutrons. The instrument has a nine-blade pyrolytic graphite (PG) analyzers. The diffraction studies were performed with 4.04Å (5 meV) neutrons, using all blades to create a 2D color plot. The sample was aligned in such a manner that the area of interest (commensurate and incommensurate magnetism) was measured in the center blade. The incommensurate part was measured in a $(0, 1 + \delta q, 0)$ scan direction. The high temperature data was subtracted to remove the $\lambda/2$ contribution from

the $(2, 0, 0)$ structural Bragg peak. For the commensurate part, the measurement was performed with a scan direction $(\delta q, 1 + \delta q, 0)$ to avoid the incommensurate contribution.

II. ACKNOWLEDGEMENTS

The Technion team was supported by the Israeli Science Foundation (ISF) and the joint German-Israeli DIP project. E.R. was partially supported by the Fonds National Suisse pour la Recherche Scientifique through Div. II and the Swiss National Center of Competence in Research MaNEP. We thank the SLS, S μ S and SINQ beam line staff at the Paul Scherrer Institute for their excellent support.

-
- [1] K. M. Shen *et al.*, Phys. Rev. B **69**, 054503 (2004).
 - [2] T. Valla, Physica C **481**, 66 (2012).
 - [3] Y. Ando, S. Komiya, K. Segawa, S. Ono, and Y. Kurita, Phys. Rev. Lett. **93**, 267001 (2004).
 - [4] F. C. Chou, F. Borsa, J. H. Cho, D. C. Johnston, A. Lascialfari, D. R. Torgeson, and J. Zioło, Phys. Rev. Lett. **71**, 2323 (1993); Ch. Niedermayer, C. Bernhard, T. Blasius, A. Golnik, A. Moodenbaugh, and J. I. Budnick, Phys. Rev. Lett. **80**, 3843 (1998).
 - [5] E. Razzoli *et al.*, New J. Phys. **12**, 125003 (2010).
 - [6] E. Razzoli, G. Drachuck, A. Keren, M. Radovich, N. C. Plumb, J. Chang, Y.-B. Huang, H. Ding, J. Mesot, and M. Shi, Phys. Rev. Lett. **110**, 047004 (2013).
 - [7] M. Fujita, K. Yamada, H. Hiraka, P. M. Gehring, S. H. Lee, S. Wakimoto and G. Shirane, Phys. Rev. B **65**, 064505 (2002).
 - [8] Matsuda, M. *et al.*, Phys. Rev. B **65**, 134515 (2002).
 - [9] J. Rameau, H.-B. Yang, and P. D. Johnson, J. Electron. Spectrosc. Relat. Phenom. **181**, 35 (2010).
 - [10] John. W. Harter, Luigi Maritato, Daniel E. Shai, Eric J. Monkman, Yuefeng Nie, Darrell G. Schlom, and Kyle M. Shen, Phys. Rev. Lett. **109**, 267001 (2012).
 - [11] Vishik *et al.*, PNAS **109** 18332 (2012).
 - [12] W. A. Atkinson J. D. Bazak, and B. M. Andersen Phys. Rev. Lett. **109**, 267004 (2012).
 - [13] J. D. Rameau, H.-B. Yang, and P. D. Johnson, J. Electron. Spectrosc. Relat. Phenom. **181**, 35 (2010).
 - [14] H.-B. Yang, J. D. Rameau, P. D. Johnson, T. Valla, A. Tselik and G. D. Gu, Nature **456**, 77 (2008).
 - [15] M. Hashimoto *et al.*, Nature Physics **6**, 414 (2010).
 - [16] A. Kanigel *et al.* Nature Physics **2**, 447 (2006).
 - [17] R. J. Gooding, N. M. Salem, and A. Mailhot, Phys. Rev. B **49**, 6067 (1994); F. Borsa, P. Carreta, J. H. Cho, F. C. Chou, Q. Hu, D. C. Johnston, A. Lascialfari, R. J. Gooding, N. M. Salem, and K. J. E. Vos, Phys. Rev. B **52**, 7334 (1995).
 - [18] Andreas Lüscher, Alexander I. Milstein, and Oleg P. Sushkov, Phys. Rev. Lett. **98**, 037001 (2007).
 - [19] E. Berg C-C Chen, and S. A. Kivelson, Phys. Rev. Lett. **100**, 027003 (2008).
 - [20] M. Shi, J. Chang, S. Pailh  s, M. R. Norman, J. C. Campuzano, M. M  nsson, T. Claesson, O. Tjernberg, A. Bendounan, L. Patthey, N. Momono, M. Oda, M. Ido, C. Mudry, and J. Mesot Phys. Rev. Lett. **101**, 047002 (2008).